

Improvement of sensitivity in high-resolution Rutherford backscattering spectroscopy

H. Hashimoto, K. Nakajima, M. Suzuki, K. Sasakawa, and K. Kimura

Citation: *Rev. Sci. Instrum.* **82**, 063301 (2011); doi: 10.1063/1.3594095

View online: <http://dx.doi.org/10.1063/1.3594095>

View Table of Contents: <http://rsi.aip.org/resource/1/RSINAK/v82/i6>

Published by the [American Institute of Physics](#).

Related Articles

A new double imaging velocity focusing coincidence experiment: i2PEPICO

Rev. Sci. Instrum. **83**, 083105 (2012)

Gamma-to-electron magnetic spectrometer (GEMS): An energy-resolved γ -ray diagnostic for the National Ignition Facility

Rev. Sci. Instrum. **83**, 10D311 (2012)

Magnetic pulser and sample holder for time- and spin-resolved photoemission spectroscopy on magnetic materials

Rev. Sci. Instrum. **83**, 063906 (2012)

Charged-particle spectroscopy for diagnosing shock pR and strength in NIF implosions

Rev. Sci. Instrum. **83**, 10D901 (2012)

Performance of a short "magnetic bottle" electron spectrometer

Rev. Sci. Instrum. **83**, 063106 (2012)

Additional information on *Rev. Sci. Instrum.*

Journal Homepage: <http://rsi.aip.org>

Journal Information: http://rsi.aip.org/about/about_the_journal

Top downloads: http://rsi.aip.org/features/most_downloaded

Information for Authors: <http://rsi.aip.org/authors>

ADVERTISEMENT



AIP Advances

Special Topic Section:
PHYSICS OF CANCER

Why cancer? Why physics? [View Articles Now](#)

Improvement of sensitivity in high-resolution Rutherford backscattering spectroscopy

H. Hashimoto,¹ K. Nakajima,¹ M. Suzuki,¹ K. Sasakawa,^{1,2} and K. Kimura^{1,a)}

¹Department of Micro Engineering, Kyoto University, Kyoto 606-8501, Japan

²Kobelco Research Institute, Inc., Takatsukadai 1-5-5, Nishi-ku, Kobe 651-2271, Japan

(Received 26 March 2011; accepted 30 April 2011; published online 1 June 2011)

The sensitivity (limit of detection) of high-resolution Rutherford backscattering spectroscopy (HRBS) is mainly determined by the background noise of the spectrometer. There are two major origins of the background noise in HRBS, one is the stray ions scattered from the inner wall of the vacuum chamber of the spectrometer and the other is the dark noise of the microchannel plate (MCP) detector which is commonly used as a focal plane detector of the spectrometer in HRBS. In order to reject the stray ions, several barriers are installed inside the spectrometer and a thin Mylar foil is mounted in front of the detector. The dark noise of the MCP detector is rejected by the coincidence measurement with the secondary electrons emitted from the Mylar foil upon the ion passage. After these improvements, the background noise is reduced by a factor of 200 at a maximum. The detection limit can be improved down to 10 ppm for As in Si at a measurement time of 1 h under ideal conditions. © 2011 American Institute of Physics. [doi:10.1063/1.3594095]

I. INTRODUCTION

High-resolution Rutherford backscattering spectroscopy (HRBS) is a powerful surface analysis technique,¹⁻⁹ which has better depth resolution compared to the conventional Rutherford backscattering spectroscopy (RBS). HRBS allows quantitative and non-destructive depth profiling of constituent elements with sub-nm depth resolution within a reasonably short measurement time (typically 10–20 min) without any special pre-treatment of the sample. A schematic drawing of the HRBS system developed at Kyoto University is shown in Fig. 1. This HRBS system has a small Cockcroft-Walton accelerator, which provides a 400 keV He⁺ ion beam with a beam current of ~50 nA. The ion beam is collimated by a series of slit systems and sent into an ultra-high vacuum scattering chamber. The ions, scattered from the specimen, are energy analyzed by a 90° sector magnetic spectrometer and detected by a one-dimensional position sensitive detector (100 mm in length) consisting of microchannel plate (MCP) and a resistive anode. The energy window and the resolution of the spectrometer are 25% and 0.1% of the analyzing energy. Depth resolution better than 0.2 nm can be achieved with this HRBS system. Although, light elements are generally difficult to analyze by RBS, the same setup can be used for high-resolution elastic recoil detection analysis which can measure depth profiles of light elements with sub-nm depth resolution.¹⁰⁻¹⁴

There are, of course, some drawbacks in HRBS. The main drawback is its relatively low elemental concentration sensitivity compared to, e.g., secondary ion mass spectrometry. Although, the sensitivity can be improved by increasing measurement time, the typical sensitivity is 100–10 000 ppm (e.g., 100 ppm for As in Si and 10 000 ppm for B in Si) in an acceptable measurement time (<1 h). This might be good enough for many applications but some ap-

plications require better sensitivity. For example, sensitivity better than 10 ppm is required in the dopant depth profiling to determine the junction depth of electronic devices. The main factor which influences the ultimate sensitivity of HRBS is the background noise in the energy spectrum. There are two major origins of the background noise in HRBS. One is stray ions scattered from the inner wall of the vacuum chamber of the spectrometer and the other is the dark noise of the MCP used in the focal plane detector of the spectrometer. In order to improve the sensitivity of HRBS, these noises should be reduced. In the present paper, we propose a method to reduce these noises. The spectrometer is modified according to the proposed method, and the performance of the modified spectrometer is examined. It is demonstrated that the background noise is reduced by factor of 200 at a maximum by this modification.

II. SENSITIVITY OF HRBS

Figure 2 shows an example of the HRBS spectrum for As-implanted Si(001) (implanted with 1 keV As⁺ ions at a fluence of 1.7×10^{14} ions cm⁻² at room temperature) observed at a scattering angle 50° under [111] channeling conditions (closed circles). The spectrum was measured with the 400 keV He ion beam of 50 nA for 1000 s. There is a small As peak at ~380 keV. The energy scale was converted to the depth scale for As and shown on the upper abscissa. The concentration of As is also shown on the right-hand ordinate. The width of the As peak is about 3 nm and the peak concentration is about 1 at. %. The background noise seems very low in this spectrum. If the vertical axis is elongated; however, a rather large background noise can be clearly seen as is shown by open circles. This background noise seriously influences the sensitivity.

The sensitivity limit of HRBS can be estimated in the following way. The net counts (the background noise is subtracted), N_{net} , of As signal and the counts of the background

^{a)}Electronic mail: kimura@kues.kyoto-u.ac.jp.

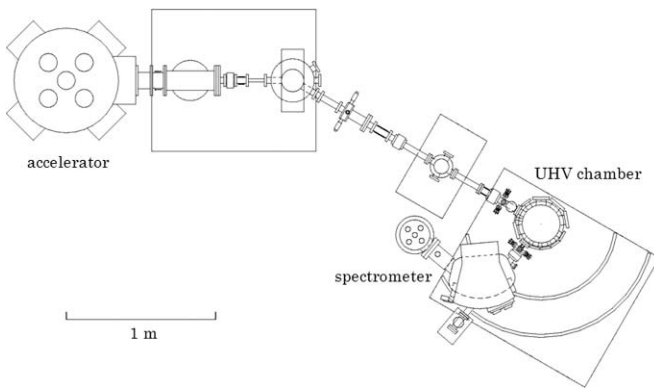


FIG. 1. Schematic drawing of a high-resolution RBS system developed at Kyoto University.

noise, N_{bg} , are proportional to the measurement time, T ,

$$N_{net} = \alpha CT, \quad N_{bg} = \beta T, \quad (1)$$

where α and β are constants and C is the concentration of As. The statistical error of N_{net} is given by

$$\Delta N_{net} = \sqrt{N_{net} + 2N_{bg}}. \quad (2)$$

If the sensitivity limit is defined by $N_{net} = \Delta N_{net}$, then the sensitivity limit is given by

$$C_{lim} = \frac{1 + \sqrt{1 + 8\beta T}}{2\alpha T}. \quad (3)$$

Figure 3 shows an example of the calculated sensitivity limit corresponding to the measurement shown in Fig. 2 (solid line). The sensitivity limit is about 200 ppm in the present case ($T = 1000$ s) and can be improved at the expense of the measurement time. For example, sensitivity limit of 10 ppm can be achieved at $T = 3.6 \times 10^5$ s (~ 4.2 days), but this is unrealistically long. Long measurement times in RBS are not just a practical inconvenience and a larger expense but may also result in increased radiation damage to the material

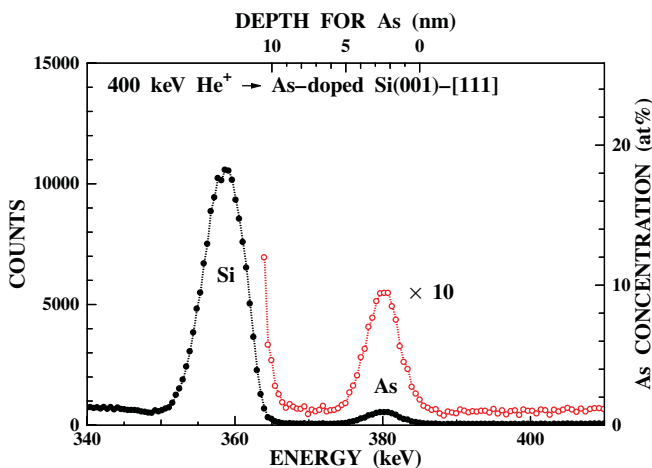


FIG. 2. (Color online) An example of the HRBS spectrum for Si(001) implanted with 1 keV As^+ at a fluence of 1.7×10^{14} ions cm^{-2} . The spectrum was measured under [111] channeling conditions with 400 keV He^+ ion beam. The depth and the concentration of As are shown on the upper abscissa and on the right-hand ordinate, respectively. A rather large background can be seen in the magnified spectrum (open circles).

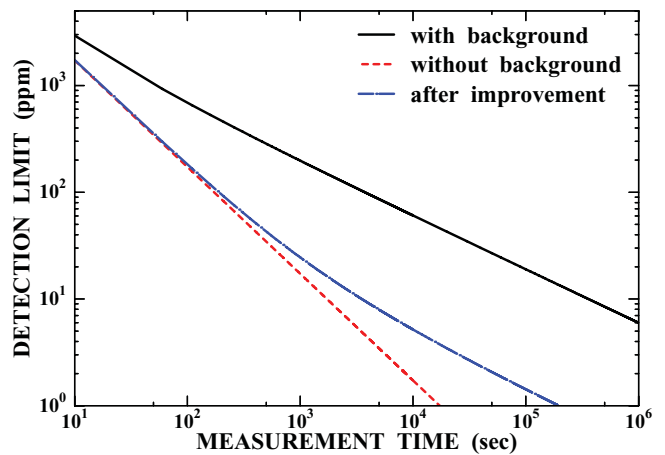


FIG. 3. (Color online) Detection limit of As in Si calculated with Eq. (3). Solid line shows the detection limit with a typical background shown in Fig. 1. Dashed line shows the detection limit without background. Dotted-dashed line shows the detection limit after the noise reduction is done as is resented in this paper.

being measured, changes in composition depth profiles. If there is no background noise, the sensitivity limit is improved as is shown by a dashed line. The sensitivity limit of 10 ppm can be easily achieved within a reasonably short measurement time (1650 s). This clearly demonstrates that the noise reduction is very effective for the improvement of the sensitivity.

III. REJECTION OF STRAY IONS

As it was mentioned above, there are two major origins of the background noise. One is the stray ions scattered from the inner wall of the vacuum chamber of the spectrometer and the other is the detector dark noise. In order to estimate the contribution of the dark noise, the spectrum was measured without the incident He beam. The observed dark-noise spectrum is shown by squares in Fig. 4 together with the spectrum observed with the He beam (closed circles). For the sake of comparison, both spectra are normalized to the measurement time. The contribution of the dark noise to the background noise is only $\sim 2\%$ at energies larger than the incident energy (400 keV), where no real signal is expected. This means that the main contribution of the background noise is the stray ions. The low (high) energy ions scattered from the sample are deflected more (less) than 90° in the spectrometer and collide with the inner wall of the vacuum chamber of the spectrometer. Some of these ions may be scattered from the inner wall towards the detector. These stray ions contribute to the background noise. An example of the trajectory of such an ion in the spectrometer is shown by a dashed line together with the trajectories of properly analyzed ions (thin solid lines) in Fig. 5. Note that the energies of these stray ions are generally much lower than those of the properly analyzed ions. In order to reject such stray ions, several barriers were installed inside the vacuum chamber of the spectrometer as is shown by thick solid lines in Fig. 5. These barriers were designed to block the stray ions but do not disturb the properly analyzed ions. In addition to these barriers, a thin Mylar foil

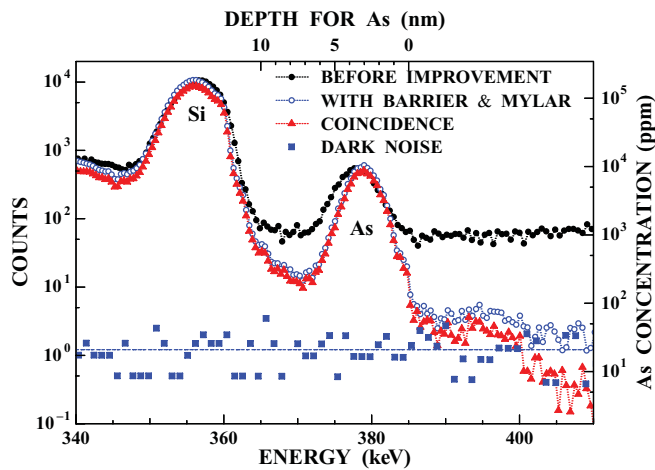


FIG. 4. (Color online) Examples of the HRBS spectra before improvement (closed circles) and after installation of barriers and the Mylar foil (open circles). The spectrum measured in coincidence with secondary electrons is shown by triangles. A spectrum measured without ion beam (dark noise) is also shown by squares. All spectra are normalized to the measurement time. The concentration of As is shown on the right-hand ordinate.

(thickness $0.5 \mu\text{m}$) was mounted in front of the MCP detector (2 mm from the MCP) to reject the low energy stray ions, which may survive the barriers. The insertion of the Mylar foil does not cause notable degradation of the energy resolution of the spectrometer because the separation between the detector and the Mylar foil is so small (2 mm).

After these modifications, the HRBS measurement was performed with the same sample and the result is shown by open circles in Fig. 4. At energies larger than the incident energy (400 keV) the background noise is reduced by a factor of 50 and is almost the same level of the dark noise of the MCP detector indicating that the stray ions are effectively rejected.

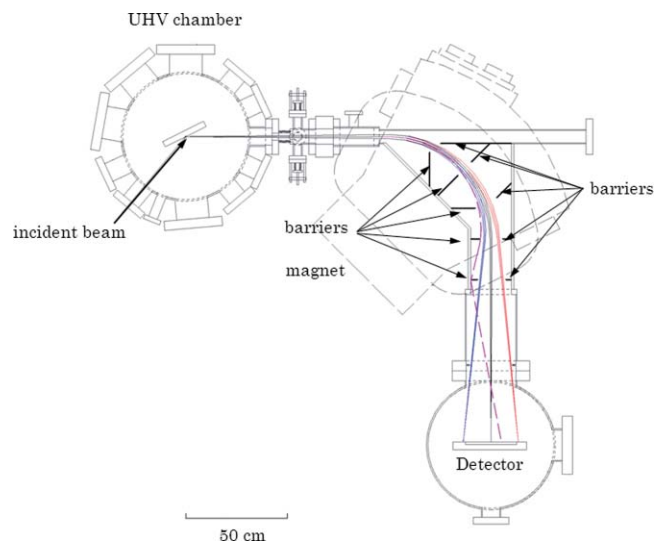


FIG. 5. (Color online) Schematic drawing of the magnetic spectrometer with barriers which were installed to reject the stray ions. An example of the trajectory of the stray ion (dashed line) and the trajectories of properly analyzed ions (thin lines) are shown.

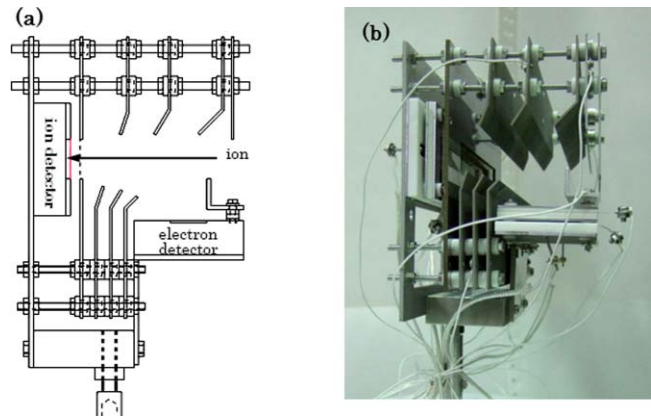


FIG. 6. (Color online) Schematic drawing and a picture of the developed detector system to reject the dark noise of the MCP detector. Secondary electrons emitted from the Mylar foil, which is mounted in front of the ion detector, are guided to the electron detector by the electrodes.

IV. REJECTION OF THE DARK NOISE OF MCP

For further improvement of the sensitivity, the reduction of the dark noise of the MCP is necessary. The origin of the dark noise of MCP is the thermal electrons emitted from the inner wall of the glass capillaries of the MCP. For the rejection of the dark noise, a new detector system was developed. Figure 6 shows a schematic drawing and a picture of the developed detector system. In addition to the MCP detector used for the ion detection, another MCP detector (electron detector) was mounted to detect secondary electrons emitted from the Mylar foil. In order to guide the secondary electrons to the electron detector, several electrodes were designed and installed between the Mylar foil and the electron detector. The secondary electrons are accelerated to 1 keV by a mesh electrode installed in front of the Mylar foil. The electrons are further accelerated up to 3 keV and guided to the electron detector. The voltages applied to the electrodes were optimized by trajectory simulation so that all secondary electrons can be detected. The electric potential distribution produced by the electrodes and examples of the secondary electron trajectories calculated using SIMION are shown in Fig. 7. All secondary electrons can be detected by the electron detector.

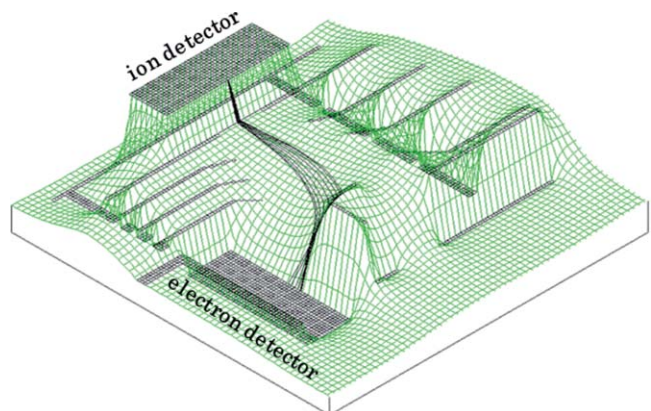


FIG. 7. (Color online) Potential distribution for electrons in the new detector system. The trajectories of secondary electrons emitted from the Mylar foil are shown.

Both ion and electron detectors have a resistive anode. Each detector puts out two signals from the both end of the resistive anode upon detection of particles. These signals are amplified by preamplifiers (113, ORTEC) and linear amplifiers (855, ORTEC) and then sent to multi-channel analyzer modules (WE7562, Yokogawa Electric Corporation), which are acquired on the personal computer (PC). The pulse height and the detection time of each signal are acquired on PC in a list mode. Position spectra and pulse height distributions of ions and electrons are extracted from the pulse height data. Using the detection-time data, the ion signals measured in coincidence with electrons are selected.

Figure 8 shows examples of the measured pulse height distributions of ion signals. The open circles show the distribution measured without coincidence. In this measurement, the beam current of the incident ions was reduced so that the performance of the present method of the dark-noise rejection can be clearly seen. There is no clear peak and the yield decreases monotonically with increasing pulse height, indicating that the dark-noise signal is dominant over the real ion signal. Only a weak shoulder can be seen at ~ 300 ch, which corresponds to the real ion signal. The closed circles show the distribution measured in coincidence with the secondary electrons. Compared to the non-coincidence result the yield is reduced at lower channels and a broad but clear peak appears at ~ 300 ch, suggesting that the dark noise is effectively removed and the distribution of the real signal is revealed.

The difference between these distributions is shown by a dashed line, which corresponds to the rejected dark-noise signals. For comparison, the pulse height distribution of the dark noise was measured for the same measurement time but without the ion beam. The result is shown by a solid line. The agreement between these two lines is reasonably good. This clearly demonstrates that the dark noise is almost completely rejected by the present method. In the conventional method

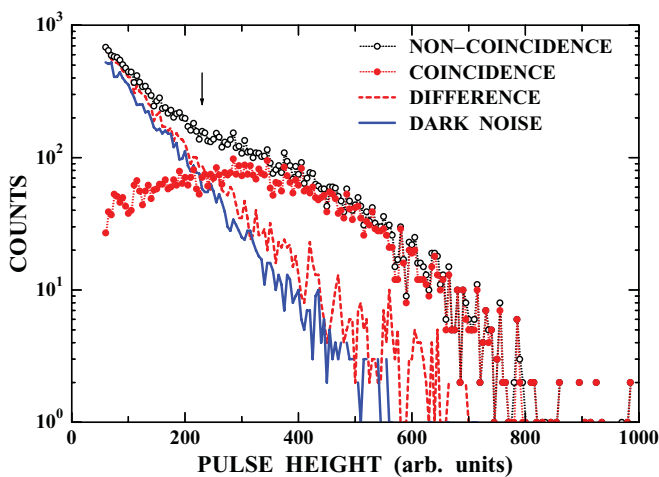


FIG. 8. (Color online) Pulse height distribution of ion signals for non-coincidence measurement (open circles) and coincidence measurement (closed circles). The difference between these distributions is shown by a dashed line. For comparison, the distribution of the dark noise is also shown by a solid line. The dark noise is effectively rejected by the coincidence measurement. In these measurements, the beam current is reduced so that the performance of this noise-rejection method can be clearly seen.

of noise rejection, signals having pulse heights lower than a certain level are rejected. An appropriate discrimination level is shown by an arrow in Fig. 8. In the present case, this simple method loses about 30% of real signals and the discriminated signals contain dark noise of 25%.

Looking at Fig. 8 closely, the distribution of the dark noise (solid line) is slightly smaller than the distribution of the removed signals (dashed line). This means that some real ion signals are rejected by the present method. This is because some ions do not produce secondary electrons upon impact on the Mylar foil and/or efficiency of the MCP detector for the secondary electron is not 100%. Due to these effects, some ion signals are rejected in the coincidence measurement.

Figure 9 shows another example of the pulse height distributions of the ion signals measured with a typical beam current in HRBS. The closed (open) circles show the coincidence (non-coincidence) result. At this beam current, the counting rate of the real ion signal is much higher than that of the dark noise. Therefore, the distributions have a clear peak even for the non-coincidence measurement. The yield ratio between the coincidence and non-coincidence measurements is also shown by triangles. The ratio is almost constant (~ 0.84) except for the very low channels. This ratio corresponds to the efficiency of the coincidence measurement. Because the efficiency of the MCP detector is typically 60%, one may wonder why the efficiency of the coincidence measurement is higher than the detector efficiency. The reason is simple, the He ion may produce multiple secondary-electrons upon impact on the Mylar foil. Figure 10 shows the pulse height distributions of the electron signals. The closed circles show the pulse height distribution of the coincidence measurement and the open circles show the distribution measured without the ion beam. In the detector chamber, there are some electrons even without the ion beam. The pulse height distribution measured without the ion beam corresponds to these electrons and represents the distribution for single-electron detection. The average pulse height of the secondary-electron signals (closed circles) is more than twice larger than that of

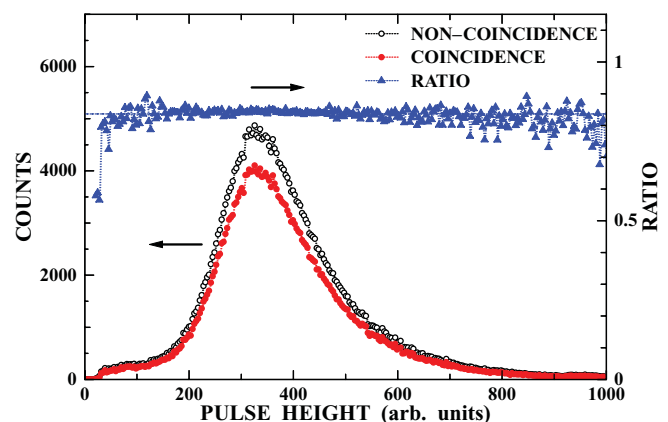


FIG. 9. (Color online) Pulse height distributions of ion signals for coincidence (closed circles) and non-coincidence (open circles) measurements with a beam current much larger than that of Fig. 8. The yield ratio between the coincidence and non-coincidence measurements is also shown by triangles. The ratio is almost constant (~ 0.84) except for the low-pulse-height region. This ratio corresponds to the efficiency of the coincidence measurement.

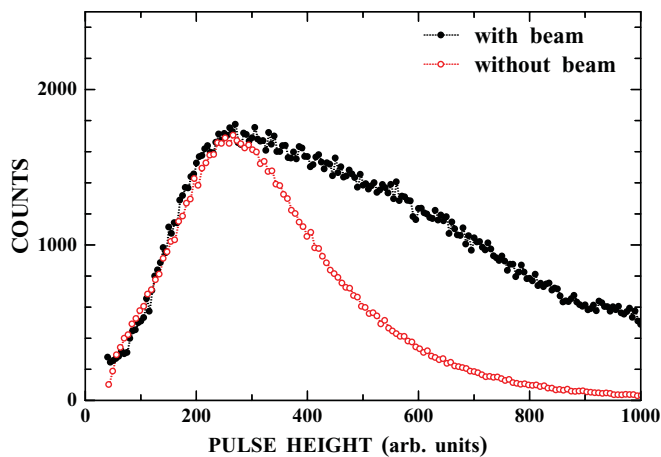


FIG. 10. (Color online) Pulse height distribution of electron signals measured in coincidence with ion signals (closed circles) and the distribution measured without the ion beam (open circles).

the single-electron detection (open circles). This confirms that the average number of secondary electrons produced by single He ion is larger than two.

V. IMPROVEMENT OF SENSITIVITY

A new measurement was performed on a different spot of the same sample (As-implanted Si(001)) using the developed detector system. The HRBS spectrum measured in coincidence with the secondary electrons is shown by triangles in Fig. 4. Compared with the spectrum measured before the improvement (closed circles), the background noise is significantly reduced, especially at the energies larger than 400 keV, where no real He signal is expected. The yield in this energy region is 200 times smaller than the background noise observed before the improvement (closed circles) and four times smaller than the dark noise. The yield between the Si and As peaks is not reduced by a factor of 200 suggesting that there are real signals corresponding to the tail of the As peak and/or other impurities. The detection limit calculated with Eq. (3) for this reduced background noise is shown by a dotted-dashed line in Fig. 3. The detection limit is about 24 ppm at $T = 1000$ s, which is one order of magnitude better than that before the improvement (200 ppm). If the measurement is performed for 3500 s the detection limit can be improved up to 10 ppm under ideal conditions. This is a promising result and may extend the application area of HRBS.

Although, the present method reduces the background noise significantly, there is still a residual background noise. In order to examine the origin of this residual background noise, measurements were performed at lower beam currents but for the same dose. If the residual background noise is ascribed to the dark noise, which somehow cannot be removed by the present coincidence method, the residual background

noise should be larger for longer measurement time. The result showed that the residual background noise does not change if the accumulated current is the same. This indicates that the residual background is not ascribed to the dark noise. The origin of the residual background might be the stray ions that cannot be removed by either the barriers or the Mylar foil. For further improvement, more careful design of the barriers should be required.

VI. CONCLUSION

A method to reduce the background noise in the high-resolution RBS was developed. The stray ions originating from the scattering at the inner wall of the vacuum chamber of the spectrometer were rejected by installation of barriers inside the spectrometer and a thin Mylar foil in front of the detector. The intrinsic background of the MCP detector, namely, the dark noise of the MCP was rejected by means of the coincidence technique. After these improvements the background noise was reduced by a factor of 200 at a maximum. This noise reduction can improve the sensitivity by one order of magnitude under ideal conditions.

ACKNOWLEDGMENTS

The authors are grateful to Dr. Tomita for providing the Mylar foil and As-implanted Si(001). This work was supported in part by Grant-in-Aid for Scientific Research from JSPS.

- ¹T. Sajavaara and K. Arstila, in *Ion Beam in Nanoscience and Technology*, edited by R. Hellborg, H. J. Whitlow, and Y. Zhang (Springer-Verlag, Berlin, 2009) p. 171.
- ²E. Bøgh, *Phys. Rev. Lett.* **19**, 61 (1967).
- ³M. Döbeli, P. C. Haubert, R. P. Livi, S. J. Spicklemire, D. L. Wethers, and T. A. Tombrello, *Nucl. Instrum. Methods B* **47**, 148 (1990).
- ⁴D. O. Boerma, F. Labohm, and J. A. Reinders, *Nucl. Instrum. Methods B* **50**, 291 (1990).
- ⁵J. Vrijmoeth, P. M. Zagwijn, J. W. M. Frenken, and J. F. Van Der Veen, *Phys. Rev. Lett.* **67**, 1134 (1991).
- ⁶T. Enders, M. Rilli, and H. D. Carstanjen, *Nucl. Instrum. Methods B* **64**, 817 (1992).
- ⁷K. Kimura, K. Ohshima, and M. Mannami, *Appl. Phys. Lett.* **64**, 2232 (1994).
- ⁸W. A. Lanford, B. Anderberg, H. Enge, and B. Hjørvarsson, *Nucl. Instrum. Methods B* **136–138**, 1177 (1998).
- ⁹R. Grötzschel, Ch. Klein, and O. Kruse, *Nucl. Instrum. Methods B* **183**, 3 (2001).
- ¹⁰M. Copel and R. M. Tromp, *Rev. Sci. Instrum.* **64**, 3147 (1993).
- ¹¹W. M. Arnoldbik, W. Wolfswinkel, D. K. Inia, V. G. G. Verleun, S. Lobner, J. A. Reinders, F. Labohm, and D. O. Boerma, *Nucl. Instrum. Methods B* **118**, 566 (1996).
- ¹²G. Dollinger, C. M. Frey, A. Bergmaier, and T. Faestermann, *Europhys. Lett.* **42**, 25 (1998).
- ¹³K. Kimura, K. Nakajima, and H. Imura, *Nucl. Instrum. Methods B* **140**, 397 (1998).
- ¹⁴K. Kimura, K. Nakajima, S. Yamanaka, M. Hasegawa, and H. Okushi, *Appl. Phys. Lett.* **78**, 1679 (2001).